AIChE

Technico-Economical Assessment of MFI-Type Zeolite Membranes for CO_2 Capture from Postcombustion Flue Gases

J. Sublet, M. Pera-Titus, N. Guilhaume, and D. Farrusseng
Institut de Recherches sur la Catalyse et l'Environnement de Lyon (IRCELYON),
UMR 5256 CNRS—Université Lyon 1, University of Lyon, 2 Av. A. Einstein, Villeurbanne 69626, France

L. Schrive
CEA Marcoule/DTCD/SPDE/Laboratoire de Fluides Supercritiques et de Membranes (LFSM),
BP 17171, 30207 Bagnols sur Cèze, France

P. Chanaud
PALL-EXEKIA, BP 1, Bazet 65460, France

B. Siret
LAB SA, 25 rue Bossuet, Lyon 69006, France

S. Durécu
TREDI, Service Recherche, BP 184, Vandoeuvre lès Nancy, 54505 France

DOI 10.1002/aic.12805
Published online December 22, 2011 in Wiley Online Library (wileyonlinelibrary.com).

A detailed survey of the effect of moisture on the CO_2/N_2 permeation and separation performance of Mobile Five (MFI) zeolite membranes in view of downstream postcombustion CO_2 capture applications in power plants and incinerators is presented. The membranes, displaying a nanocomposite architecture, have been prepared on α-alumina tubes by pore-plugging hydrothermal synthesis at 443 K for 89 h using a precursor clear solution with molar composition 1 SiO_2:0.45 tetrapropylammonium hydroxide:27.8 H_2O. The synthesized membranes present reasonable permeation and CO_2/N_2 separation properties even in the presence of high water concentrations in the gas stream. A critical discussion is also provided on the technico-economical feasibility (i.e., CO_2 recovery, CO_2 purity in the permeate, module volume, and energy consumption) of a membrane cascade unit for CO_2 capture and liquefaction/supercritical storage from standard flue gases emitted from an incinerator. Our results suggest that the permeate pressure should be kept under primary vacuum to promote the CO_2 driving force within the membrane. *AIChE J*, 58: 3183–3194, 2012
Keywords: MFI membrane, carbon dioxide, moisture, incineration, CO_2 capture

Introduction

Climate change due to anthropogenic CO_2 emissions is one of the greatest environmental, social, and economic threats facing the Earth in the forthcoming decades. To mitigate the warming effect on climate, a net reduction of CO_2 emissions is imperative. CO_2 capture, transport, and long-term storage (CCS) is visualized as a promising strategy for cutting CO_2 emissions at short and mid terms. Among the three steps of the CCS chain, CO_2 capture is by far the most expensive one, accounting for 50–90% of the overall chain cost, this also depending strongly on the emission source.[1]

In essence, CO_2 capture from fossil fuel combustion can be achieved following three different strategies[2]: (1) oxy-combustion (combustion performed with pure oxygen), (2) precombustion (decarbonatation before combustion), and (3) postcombustion (end-of-pipe CO_2 recovery). The strategic target separations to make these processes feasible are: O_2/N_2 for oxycombustion, CO_2/H_2 for precombustion, and CO_2/N_2 for postcombustion CO_2 capture. The third possibility is the most challenging because a diluted (<12 v/v % CO_2), low-pressure (1–3 bar), and wet (3–10 v/v % water) CO_2/N_2 mixture has to be treated. Nevertheless, it corresponds to the most widely extended industrial application, showing the advantage of being compatible with a retrofit strategy.

Chemical absorption with mono-, di-, and tri-ethanol-amines or variants using packed towers or membrane contactors, constitutes the best available technology for CO_2 capture from flue gas steams in large emission sources. The absorbed gas is further liberated in a separate vessel by raising the temperature and/or lowering the pressure above the solution, the regenerated solution being recirculated to the absorption unit. The main shortcoming of this technology is ascribed to the extremely high-energy demands, lying in the range 4–6 GJ/t CO_2 avoided (including heating and electrical consumption),[3,4] as well as to amine losses and degradation

Correspondence concerning this article should be addressed to M. Pera-Titus at marc-pera-titus@ircelyon.univ-lyon1.fr.

in the presence of O_2 and SO_2. Alternative processes based on pressure and thermal swing adsorption relying on well-engineered solid adsorbents have also been considered for CO_2 separation.[5,6]

In addition to these technologies, membrane-based processes have gained increasing interest in recent times to make postcombustion CO_2 capture more energy efficient and cost effective. According to Favre,[7] membranes could potentially compete with chemical absorption in terms of energy demands (<0.75 GJ/t CO_2 avoided) if the CO_2 content in the feed exceeds 20 v/v %. At lower compositions, postcombustion CO_2 capture might be only feasible at the level of 1–2 GJ/t CO_2 avoided. The use of vacuum operation in the permeate combined with moderate compression in the feed might reduce the energy requirements to a level <1 GJ/t CO_2 avoided.

Polymeric membranes have been widely investigated for gas separation applications. Nevertheless, their practical use for CO_2 capture has often been limited due to their insufficient thermal, mechanical, and chemical stability and to their low permeances. As a matter of fact, a CO_2/N_2 permselectivity of 50 associated to a CO_2 permeance of 3 nmol m^{-2} s^{-1} Pa^{-1} (1-μm thick) can be taken as the present upper limit of glassy polymeric membranes.[3,8] Recent advances on rubbery polymeric membranes offer materials with improved CO_2 permeances (up to three orders of magnitude higher),[9,10] but most often at the expenses of lower selectivity toward CO_2 separation, involving high energy requirements (>3.5 GJ/t CO_2 avoided).[9] Moreover, although emerging hybrid or mixed-matrix membranes (e.g., polymer/zeolite,[11,12] polymer/MCM-41,[11,13] polymer/MOF[14]) might offer some improvements, these materials do not appear to constitute realistic candidates for chemical absorption or gas adsorption in industrial applications.

Although there is still plenty of room for improving the separation capacity and stability of polymeric membranes in view of realistic postcombustion CO_2 separation applications (Polaris™ membranes from MTR are a recent example),[10] we concentrate our attention in this study on the use of ceramic membranes as alternative candidates for CO_2 separation. In particular, zeolite membranes have attracted great interest in the last two decades, because they are capable of separating compounds by combination of molecular sieving, selective adsorption, and differences in surface diffusion rates.[15-17] Most zeolite membranes reported in the literature are stable with respect to temperature and pressure, but contaminant species can significantly affect their permeation properties. Moreover, the manufacture of large surface defect-free zeolite membranes is a major engineering challenge, because very thin supported layers often present defects (cracks). Our group has concentrated on routes using tubes combined with new ideas for zeolite growth (pore-plugging approach) reducing both the cost and complexity of the systems as well as improving at the same time the membrane reproducibility.[18-20]

Despite the promising CO_2/N_2 separation results reported in the literature on MFI,[21-24] FAU,[25-30] SAPO-34,[31-35] DD3R,[36,37] and T[38] zeolite membranes, care should be taken when analyzing these data due to a lack of tests carried out under real postcombustion CO_2 capture conditions. Indeed, most of these studies do neither provide much insight into the hydrothermal stability of the membrane materials, nor into their CO_2 permeation and separation properties in the presence of moisture. Nevertheless, a reduced number of studies have appeared tackling these questions. Poshusta et al.[39] reported fairly stable CO_2 permeances and CO_2/CH_4 separation factors within high-quality SAPO-34 membranes after water introduction. The membranes suffered however from ageing after long exposure to a wet atmosphere, this phenomenon being accelerated in the presence of nonzeolite pores by increasing the water accessibility to SAPO-34 crystals. Himeno et al.[40] published a comprehensive study on high-quality DD3R membranes pointing out a remarkable decrease of the CO_2 permeance (ca. 40%) in the presence of a moisture-saturated stream, the CO_2/CH_4 separation factor being enhanced about 50%. Gu et al.[41] also reported a drastic reduction of steady-state CO_2 and N_2 permeances at 473 K (more than one order of magnitude) for partial pressures >20 kPa. Beyond this level, the CO_2/N_2 separation factor showed a progressive decrease from a maximum value about 4.5.

In the particular case of MFI-type zeolite membranes, Funke et al.[42] reported no permanent effect of water vapor on the pure permeation performance of ZSM-5 membranes. Although the pure N_2 and SF_6 permeances decreased after humification of the feed stream (61% for N_2 and 16% for SF_6), the initial values were recovered after water removal. Bernal et al.[43] explored the room-temperature CO_2/N_2 separation performance (equimolar mixture) of B-ZSM-5 membranes saturated with water vapor. The CO_2 permeation fluxes decreased about 54% and 29% for a feed pressure of 1.7 and 2.2 bar, respectively, without use of a sweep gas in the permeate stream, the separation factor keeping essentially unchanged. Finally, Shin et al.[44] reported an increase of the membrane selectivity in the separation of a moisture-saturated equimolar CO_2/N_2 mixture by a surface-modified ZSM-5 membrane. The room-temperature CO_2/N_2 separation factor was about 50 for dry mixture and about 60 for wet mixture steady-state separation. It was believed that water blocked partially both the MFI adsorption sites and the intercrystalline nonzeolite pores, overcoming N_2 permeation and thus increasing the CO_2/N_2 separation factor.

In this study, we describe the application of MFI-alumina membranes with nanocomposite architecture prepared in our laboratory for postcombustion CO_2 capture in the presence of moisture. Although these materials do not offer *a priori* the most attractive combination of adsorption/diffusion properties for CO_2 separation unlike FAU- or DDR-type membranes (see for instance Ref. 45), nanocomposite MFI membranes offer some additional major advantages: (1) the synthesis of the material is highly reproducible and easier to upscale (see Ref. 19), (2) high CO_2 permeances can be attained even in the presence of water vapor compared to more hydrophilic zeolite materials (e.g., FAU), reaching the level of 0.7 μmol m^{-2} s^{-1} Pa^{-1} for MFI-alumina hollow fibers,[46] and (3) the materials show a high hydrothermal resistance. These three aspects, in addition to appropriate CO_2/N_2 separation factors, are imperative for the industrial implementation of membrane devices. Our aim here is to assess for experimental operation conditions allowing moderate gas permeance reduction upon water introduction on these materials and operation under primary vacuum for the permeate stream to promote the CO_2 driving force within the membranes. On the basis of these results, a technico-economical analysis will be carried out relying on a membrane cascade configuration for attaining an overall CO_2 removal

target of at least 75% of the inlet value and a CO_2 purity of at least 95% in the downstream permeate current, allowing further CO_2 liquefaction/supercritical storage. A case study is proposed for stationary postcombustion CO_2 capture in incineration plants.

Experimental

Materials

The MFI membranes were prepared on porous asymmetric 15-cm-long tubular supports with 7 mm i.d. and 10 mm o.d. provided by Pall Exekia (Membralox T1-70). The quality of the supports was inferred from the values of the first bubble point pressure under ethanol, higher than 80 kPa in all cases. The supports consisted of three α-alumina layers with mean pore size and thickness decreasing from the outer to the inner side of the tubes, with the following pore size sequences (as given by the provider): 12–0.8–0.2 μm and 12–0.8–0.1 μm (top-layer thickness: 10 μm in both cases). The first 12-μm layer had a porosity of 33%, whereas that of the other two layers was 30%. Both ends of the supports were enameled (1.5 cm at each side) for sealing purposes, defining a permeation length of 12 cm.

Some supported MFI samples were also prepared on alumina hollow fibers (1.67 mm o.d., 1.15 mm i.d., 250 mm length, surface pore size <0.5 μm, and an overall porosity of 43%) for CO_2 and water adsorption tests. These samples were crushed after synthesis for analysis.

Aerosil 380 (fumed SiO_2), supplied by Sigma-Aldrich, was used as silica source. Tetrapropylammonium hydroxide (TPAOH, 1 M) was used as template agent. The gases (He, Air, N_2, O_2, and CO_2, purity > 99.9999%) were supplied by Air Liquide.

Membrane preparation

The nanocomposite MFI-alumina membranes were prepared by pore-plugging interrupted hydrothermal synthesis in a Teflon-lined autoclave (15 mL) at 443 K for 89 h using a precursor solution with varying molar composition 1 SiO_2:0.45 TPAOH:27.8 H_2O during 3 days at room-temperature under mild stirring. More details on the synthesis protocol can be found in previous publications.[19,20]

After the tests, the membranes were washed with distilled water until neutral pH, dried at 373 K for 12 h, and calcined at 773 K for 6 h with heating and cooling ramps of 1 K/min.

Physical characterization

Inductive coupled plasma atomic emission spectroscopy (ICP-AES) was used to quantify the overall amount of Si and Al on the membranes, and zeolite powder collected from the bottom of the autoclave after hydrothermal synthesis using a Perkin Elmer M1100 spectrometer. For Si analysis, the sample was fused in $Li_2B_4O_7$ using a Pt-Au crucible by heating up to 1273 K and then dissolving in HCl (20 wt %).

The zeolite powder collected from the bottom of the autoclave and crushed hollow fibers were analyzed by x-ray diffraction using a Philips PW1050/81 diffractometer (Cu $K_{\alpha 1+2}$ radiation) to assess for the nature of the crystallized materials.

CO_2 and water isotherms were measured on a BelSorp HP and a BelSorpMax microvolumetric apparatus, respectively. Before the adsorption measurements, the samples were desorbed at 523 K and 10^{-5} torr for 4 h to remove adsorbed species.

Pure hydrogen permeation and butane/H_2 separation tests

The quality of the as-synthesized MFI-alumina membranes was evaluated first by a pure H_2 permeance test at room-temperature in dead-end mode using a 303-kPa transmembrane pressure. The H_2 permeance was measured using a DryCal piston volumetric flowmeter connected to the permeate stream of the membrane. Subsequently, *n*-butane/H_2 equimolar separation tests were carried out in Wicke-Kallenbach (WK) mode (i.e., $\Delta P \approx 0$). These tests were carried out at different temperatures by feeding 8 mL(STP)/min of *n*-butane and H_2 each diluted in 64-mL(STP)/min N_2 to the membrane module, whereas 80-mL(STP)/min N_2 were swept over the membrane on the permeate side. The pressure at both sides was kept at 125 kPa using two regulation valves.

The MFI effective thickness of the membrane materials was estimated by fitting the Maxwell-Stefan (MS) equation defined by Eq. 1 to the experimental trends of the pure H_2 permeance with temperature

$$N = \frac{c_{sat}\rho\varepsilon D_o^{\infty}}{\tau\ell}\ln\left[\frac{1+\frac{P_R}{P^o}\exp\left(\frac{\Delta S_{ads}^o}{R}-\frac{\Delta H_{ads}^o}{RT}\right)}{1+\frac{P_P}{P^o}\exp\left(\frac{\Delta S_{ads}^o}{R}-\frac{\Delta H_{ads}^o}{RT}\right)}\right]\exp\left[-\frac{E_D}{RT}\right] \quad (1)$$

with (parameter values for H_2 taken from Ref. 47): R, ideal gas constant (8.314 J mol^{-1} K^{-1}); c_{sat}, concentration of the gas in MFI crystals (5.4 mol/m^3); ρ_{MFI}, skeletal MFI density (1700 kg/m^3); ε, porosity of MFI membrane (0.13); D_0^{∞}, MS diffusivity at zero coverage (1.8×10^{-8} m^2/s); τ, tortuosity (1.2); ℓ, equivalent MFI thickness (m, fitted parameter); P_R, retentate pressure (Pa); P_P, permeate pressure (Pa); P^o, reference to atmospheric pressure (101325 Pa); ΔS_{ads}^0, standard entropy of adsorption (−43 J mol^{-1} K^{-1}); ΔH_{ads}^0, standard enthalpy of adsorption (−5900 J/mol); and E_D, activation energy for diffusion (2000 J/mol).

Mixture CO_2/N_2 permeation tests

The calcined membranes were mounted in a stainless steel module and sealed with graphite o-rings. Before the gas permeation tests, the membranes were subjected to an *in situ* pretreatment at 673 K for 6 h using a heating ramp of 1 K/min under a 20 mL(STP)/min He sweep flowrate at both membrane sides to remove adsorbed moisture and organic vapors on the guidance of a previous study.[48] After 4 h, the temperature was decreased to room temperature and then stabilized to the desired value to carry out the permeation tests.

Figure 1 shows a scheme of the setup used for carrying out the CO_2/N_2 permeation and separation tests in the presence of moisture. Briefly, gas flowrates and feed compositions were regulated using mass flow controllers (Brooks, type 5850S). An equimolar CO_2/N_2 mixture (200–500 mL(STP)/min) was fed to the inner side of the membrane. The permeate was either swept with an He flow (60–80 mL(STP)/min) or submitted to primary vacuum (10–30 mbar) using a membrane pump (Adixen).

The composition of the feed, retentate, and permeate streams was analyzed online using an Agilent 3000A μGC equipped with two columns (PPU + MS5A and PPQ + PPU) and two thermal conductivity detectors using Ar and He as carrier gases, respectively. Two regulation valves at the outlet of the retentate and permeate streams were used to adjust the feed and transmembrane pressures, respectively. The desired water relative humidity in the feed stream was introduced by heating a pressurized liquid water stream with

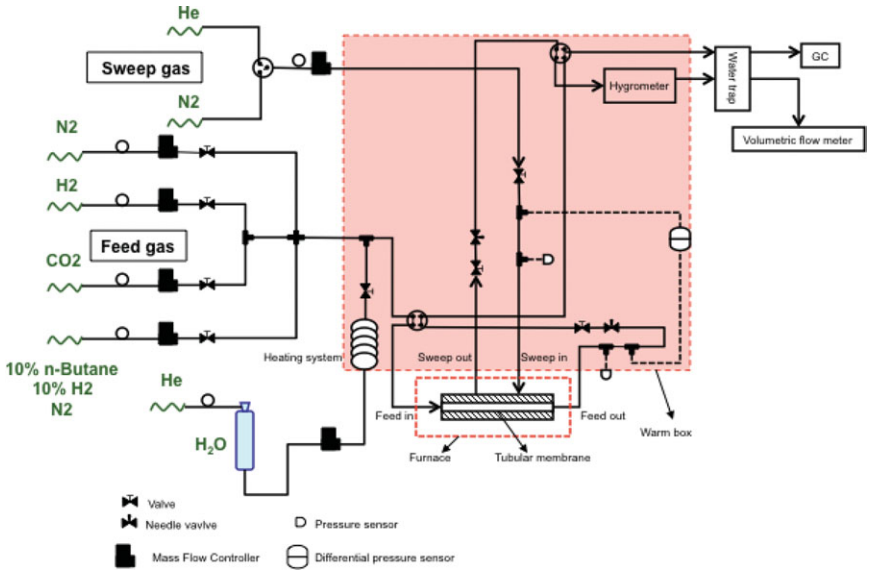

Figure 1. Experimental setup for CO_2/N_2 permeation and separation tests in the presence of moisture.

[Color figure can be viewed in the online issue, which is available at wileyonlinelibrary.com.]

the corresponding flowrate controlled using a liquid mass flow controller (Bronkhorst Hi-Tech). A hygrometer equipped with a probe was used for monitoring the relative humidity in the feed and permeate streams.

The permeance of a target species was defined as the permeation flux divided by its corresponding log-mean differential partial pressure, whereas the separation factor ($Sf_{i/j}$) was defined as the enrichment factor of one component to another in the permeate, as compared with the feed composition ratio

$$Sf_{i/j} = \left(y_i/y_j\right)_{\text{permeate}} \Big/ \left(x_i/x_j\right)_{\text{feed}} \tag{2}$$

where x_i and x_j as well as y_i and y_j are the molar fractions of species i and j in the retentate and permeate streams, respectively.

Results and Discussion

Quality of the synthesized MFI-alumina membranes

Table 1 collects the room-temperature pure H_2 permeance and *n*-butane/H_2 separation factor measured for the different membranes prepared in this study as primary indicators of membrane quality. The listed values reflect optimal membrane quality in terms of a reduced density of intercrystalline defects in the intergrown MFI layer. Let us recall from previous studies on nanocomposite MFI-alumina tubular membranes that membranes showing room-temperature pure H_2 permeances <0.4 μmol m^{-2} s^{-1} Pa^{-1} and *n*-butane/H_2 separation factors >25 are usually considered acceptable for gas separation purposes.[18,20]

Figures 2 and 3 show an example of evolution of the pure H_2 permeation flux and *n*-butane/H_2 equimolar mixture permeation and separation properties, respectively, as a function of temperature for sample M2. The H_2 flux shows a continuous decrease with temperature without indication of permeance increase beyond 600 K, as expected for a nanocomposite architecture,[18,47] opposing to the general trend commonly found in film-like MFI membranes. The H_2 evolution trend with temperature allows the measurement of the effective MFI thickness of the nanocomposite materials through MS fitting (Eq. 1). The computed MFI thicknesses for the different materials fall into the range 0.55–2 μm.

The *n*-butane flux shows a characteristic maximum at 430 K, whereas the *n*-butane/H_2 separation factor shows a decreasing trend with temperature from a value of 25–57 (preferential *n*-butane permeation) at room temperature to <1 (preferential H_2 permeation) beyond 600 K. The flux pattern with temperature is in good keeping with an adsorption-driven permeation mechanism, confirming the absence of a significant amount of defects in the MFI layer.

CO_2/N_2 mixture permeation and separation under He sweep gas and vacuum pressure

The membrane samples prepared in this study show pure CO_2 and N_2 permeance values that are comparable to the

Table 1. Membrane Quality of the Different Membrane Materials Prepared in This Study: Room-Temperature *n*-Butane/H_2 Separation Factor and Pure H_2 Permeance

			Dry Gas*		Humid Gas*,†	
Reference	SF *n*-Butane/H_2	H_2 Permeance (μmol m^{-2} s^{-1} Pa^{-1})	CO_2 Permeance (μmol m^{-2} s^{-1} Pa^{-1})	CO_2/N_2 Separation Factor	CO_2 Permeance (μmol m^{-2} s^{-1} Pa^{-1})	CO_2/N_2 Separation Factor
M1	25	0.17	0.44	4.0	–	–
M2	57	0.31	0.28	1.8	0.10	3.3
M3	38	0.12	0.31	1.5	0.12	4.0
M4	34	0.23	0.35	1.6	0.045	9.5

*T = 323–337 K, 10:90 CO_2/N_2, P_{feed} = 303–404 kPa, ΔP = 0–2.5 kPa, sweep flowrate = 60–90 mL(STP)/min.
†Humidity = 1–3 v/v % water.

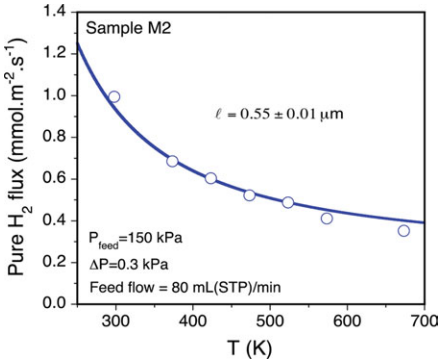

Figure 2. Evolution of the pure H_2 permeance as a function of temperature for sample M2.

The curve corresponds to the fitting to Eq. 1. [Color figure can be viewed in the online issue, which is available at wileyonlinelibrary.com.]

highest values reported in the literature on conventional film-like MFI membranes,[21] probably due to similar MFI effective thickness (<8 μm). Indeed, pure CO_2 and N_2 permeances of 0.16 and 0.084 μmol m^{-2} s^{-1} Pa^{-1}, respectively, have been obtained for sample M2. These permeance values translate into a CO_2/N_2 ideal permselectivity of about 1.9, which is higher than the corresponding Knudsen selectivity $\approx$ 0.8. The amount of large intercrystalline defects of the synthesized MFI material is low, as inferred from the low viscous contribution to N_2 permeance after calcination (lower than 2%), obtained from the slope of N_2 permeance with the average pressure (not shown).

The different membrane materials have been submitted to mixture CO_2/N_2 separation both by subjectting the permeate stream to a He sweep gas (WK configuration) and to primary vacuum. The former conditions aim at promoting the transmembrane CO_2 partial pressure within the membrane material without need of pressurizing the feed stream to very high values. These conditions are especially attractive for CO_2 separation from highly diluted streams, as is the case often encountered in postcombustion CO_2 capture applications. The use of a He sweep gas, though discouraged for industrial applications, is however useful for simulating the action of vacuum

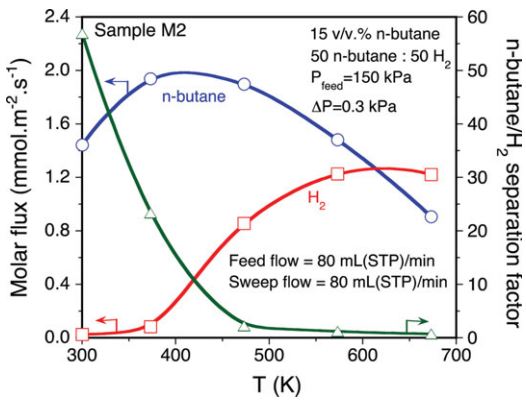

Figure 3. Evolution of *n*-butane and H_2 molar fluxes with temperature in the separation of an *n*-butane/H_2 equimolar mixture for sample M2.

The curves are a guide to the eye. [Color figure can be viewed in the online issue, which is available at wileyonlinelibrary.com.]

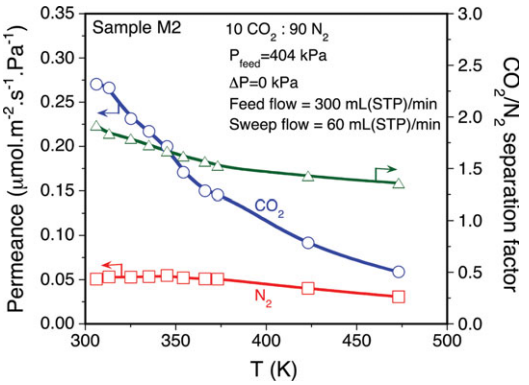

Figure 4. Evolution of the CO_2/N_2 separation factor and mixture CO_2 and N_2 permeances with temperature for sample M2 in the separation of a 10:90 CO_2/N_2 mixture under the presence of a He sweep gas in the permeate stream.

The curves are a guide to the eye. [Color figure can be viewed in the online issue, which is available at wileyonlinelibrary.com.]

and for comparison with CO_2 permeation and separation data available in the literature. We have verified the absence of He counterdiffusion from the permeate to the retentate stream in such tests.

Figure 4 plots the evolution of the CO_2/N_2 mixture permeation and separation performance as a function of temperature for membrane M2 by submitting the permeate stream to a He sweep flowrate. The membrane shows a CO_2 permeance up to 0.28 μmol m^{-2} s^{-1} Pa^{-1} at near room-temperature and 10:90 CO_2/N_2 feed composition, the CO_2 permeance showing a characteristic decreasing trend with temperature, as expected from an adsorption-driven permeation mechanism. A maximum CO_2/N_2 separation factor about 1.7 is achieved at near room-temperature.

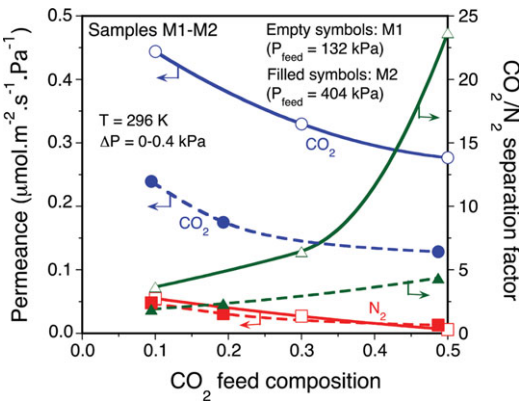

Figure 5. Evolution of the CO_2/N_2 separation factor and mixture CO_2 and N_2 permeances with the feed composition for samples M1 and M2 under the presence of a He sweep gas in the permeate stream.

Other experimental conditions: (M1) feed flowrate, 200 mL(STP)/min; He sweep flowrate, 80 mL(STP)/min; (M2) feed flowrate, 200 mL(STP)/min; He sweep flowrate, 60 mL(STP)/min. The curves are a guide to the eye. [Color figure can be viewed in the online issue, which is available at wileyonlinelibrary.com.]

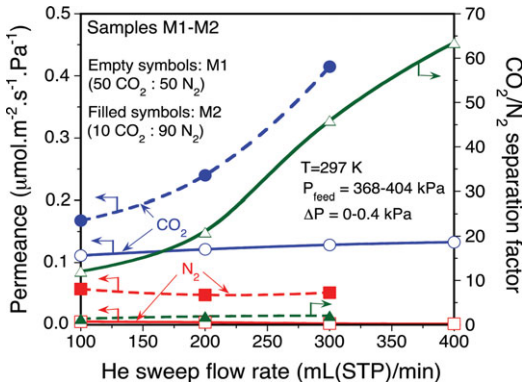

Figure 6. Evolution of the CO_2/N_2 separation factor and mixture CO_2 and N_2 permeances with the He sweep flowrate for samples M1 and M2.

Other experimental conditions: feed flowrate, 1000 mL(STP)/min (M1) and 90 mL(STP)/min (M2). The curves are a guide to the eye. [Color figure can be viewed in the online issue, which is available at wileyonlinelibrary.com.]

Figures 5 and 6 plot the evolution of the CO_2/N_2 mixture permeation and separation performance as a function of the CO_2 feed composition and the He sweep flowrate for membranes M1 and M2, respectively. Although the CO_2 and N_2 permeation fluxes increase with the CO_2 feed composition due to an increase of the driving force within the membrane (see Figure 5), the corresponding permeances show a marked reduction on the basis of a more pronounced increase of logarithmic mean partial pressures. The CO_2/N_2 separation factor shows, however, a prominent increase with the CO_2 feed composition, achieving a value as high as 23 for an equimolar feed for membrane M1, due to a comparably higher driving force for CO_2.

The CO_2 permeance is dramatically promoted with the He sweep gas flowrate for diluted streams, whereas it keeps practically unchanged for equimolar CO_2/N_2 mixtures (see Figure 6). The former trend can be attributed to a comparably higher effect of reduced CO_2 permeate partial pressures on promoting the driving force within the membrane material. Indeed, at low CO_2 concentrations, the CO_2 loading in the feed side of membrane M1 is expected to be modest. This trend is accompanied by a pronounced increase of the CO_2/N_2 separation factor with the He sweep flowrate, reaching a value higher than 60 for a 400-mL(STP)/min He flowrate. At higher CO_2 feed concentrations, however, the much higher CO_2 driving force within the membrane is expect to compensate the positive effect of the He sweep gas flowrate on the membrane permeation and separation properties.

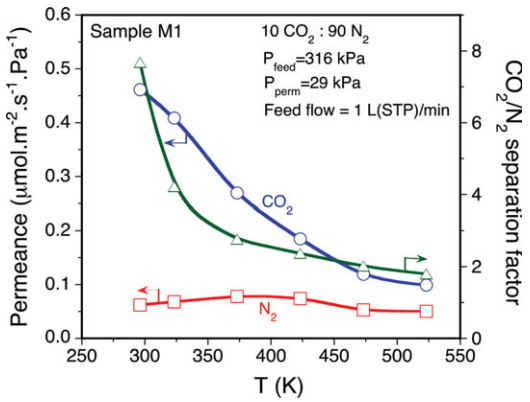

Figure 7. Evolution of the CO_2/N_2 separation factor and mixture CO_2 and N_2 permeances with temperature for sample M1 in the separation of a 10:90 CO_2/N_2 mixture under the presence of vacuum in the permeate stream.

The curves are a guide to the eye. [Color figure can be viewed in the online issue, which is available at wileyonlinelibrary.com.]

Figures 7 and 8 plot the evolution of the CO_2/N_2 mixture permeation and separation performance as a function of temperature and the transmembrane pressure, respectively, for membrane M1 keeping the permeate stream under vacuum (47–293 kPa). The membrane shows a CO_2 permeance up to 0.5 μmol m^{-2} s^{-1} Pa^{-1} at near room-temperature and 10:90 CO_2/N_2 feed composition. This value is much higher than the permeances commonly found when submitting the permeate to a sweep gas, most probably due to a much higher CO_2 driving force within the membrane. Furthermore, the CO_2 permeance shows a decreasing trend with temperature (see Figure 7), as in the case found when submitting the permeate to a He sweep flow (see Figure 4). A maximum CO_2/N_2 separation factor about 7 is achieved at near room-temperature.

The CO_2 permeance tends to be promoted with the transmembrane pressure, this increase being more pronounced when decreasing the CO_2 feed concentration (cf. the trends plotted in Figure 5 for 10:90 and 50:50 CO_2/N_2 feed compositions on membranes M1 and M2, respectively). The N_2 permeance is slightly promoted with the transmembrane pressure for a 10:90 CO_2/N_2 feed composition on membrane M2, whereas the trend is slightly decreasing for a 50:50 CO_2/N_2 feed composition on membrane M1. The CO_2 and N_2 permeation trends at both conditions translate into a moderately positive evolution of the CO_2/N_2 separation factor with the transmembrane pressures at lower CO_2 compositions, whereas the trend shows a decreasing trend for an equimolar CO_2/N_2 mixture.

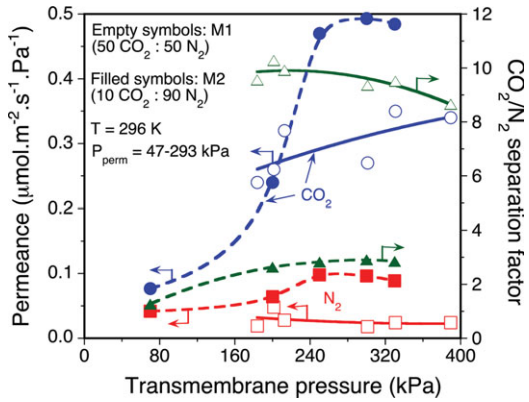

Figure 8. Evolution of the CO_2/N_2 separation factor and mixture CO_2 and N_2 permeances with the transmembrane pressure for samples M1 and M2 under the presence of vacuum in the permeate stream.

Other experimental conditions: feed flowrate, 1000 mL(STP)/min (M1) and 500 mL(STP)/min (M2). The curves are a guide to the eye. [Color figure can be viewed in the online issue, which is available at wileyonlinelibrary.com.]

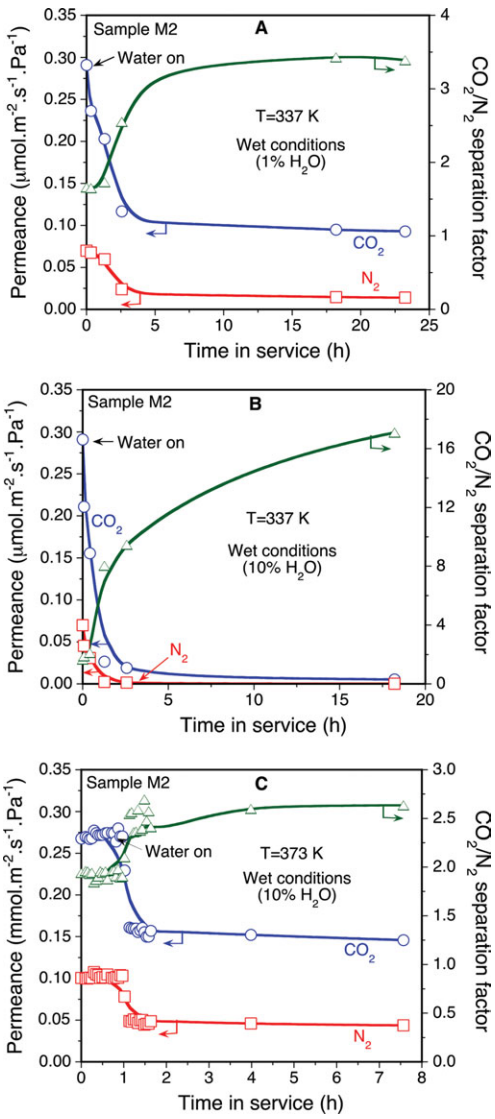

Figure 9. Time evolution of CO_2 and N_2 permeances and CO_2/N_2 separation factor for sample M2 in the presence of 1 v/v % (top) and 10 v/v % (middle and bottom) water concentrations at 337–373 K.

Other experimental conditions: feed composition 10:90 CO_2/N_2; feed pressure, 404 kPa; transmembrane pressure, 0 kPa; feed flowrate, 300 mL(STP)/min; He sweep flowrate, 60 mL(STP)/min. [Color figure can be viewed in the online issue, which is available at wileyonlinelibrary.com.]

Effect of moisture on the CO_2 permeation and separation properties

Figures 9–11 plot the evolution of the CO_2 and N_2 permeances and CO_2/N_2 separation factor within membranes M2–M4 as a function of time at 303–373 K after the introduction of 1–10 v/v % humidity in the gas stream. Table 1 provides comparative data on the different membranes. As can be deduced from these figures, membrane permeation appears to be suppressed for highly humid gases (10 v/v % concentration) at 337 K (see Figure 9B). In contrast, when submitting the membranes either to lower water concentrations (1–3 v/v %, Figures 9A, 10, and 11) at 323–337 K, or to higher temperatures, still keeping high water concentrations (i.e., ca. 373 K at 10 v/v % water concentration, Figure 9C), water does not completely impede the membrane permeation performance. In the former case, the CO_2 and N_2 permeances show a steady-state decrease of about 50–60% when incorporating water to the feed stream, membranes M2–M4 still exhibiting a reasonably high CO_2 permeance at 323 K under 2–3 v/v % water humidity at a level about 0.2 μmol m^{-2} s^{-1} Pa^{-1}. At higher temperatures, the CO_2 and N_2 permeances show a more moderate reduction of about 40% when incorporating water to the feed stream, membrane M2 still showing a CO_2 permeance at a level about 0.15 μmol m^{-2} s^{-1} Pa^{-1} at 373 K (see Figure 9C). In all cases, water exerts a positive effect on the CO_2/N_2 separation factor, especially for membrane M2 at 337 K and 10 v/v % water concentration, this attaining a value higher than 15 after 17-h operation from an initial value about 1.7.

The fact that CO_2/N_2 permeation within MFI-alumina membranes is not completely blocked in the presence of water vapor can be attributed to a moderate water adsorption in micropores (sitting near cations). This image is compatible to the water adsorption pattern on MFI powders, showing a Type II behavior differing from the characteristic Type I (pore filling) observed for CO_2 adsorption (see Figure 12). The membranes display reasonably high permeances at 373 K in the presence of high water concentrations (>10 wt %), these being almost unaffected in the range beyond 2 wt %. Although we do not exclude the formation of water multilayers on the external membrane surface at high water concentrations after capillary condensation in defective mesopores, these might still allow the accessibility of CO_2 molecules to the zeolite channels. The increase of the CO_2/N_2 separation factors in the presence of water can be explained on the basis of defective pore blockage. Moreover, a positive interaction between CO_2 and water, most probably through the formation of (bi)carbonate species and/or CO_2 stabilization by hydrogen bonds cannot be ruled out.

Discussion: Technico-Economical Assessment of MFI Membranes for Postcombustion CO_2 Capture

In light of the results presented above, we discuss in this section the suitability of the MFI-alumina membranes developed in our laboratory for postcombustion CO_2 capture in power plants and incinerators in terms of energy costs and

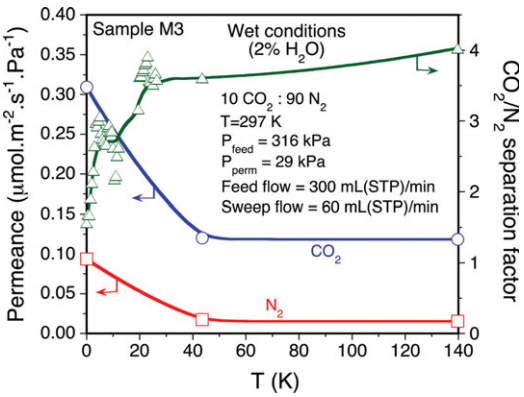

Figure 10. Time evolution of CO_2 and N_2 permeances and CO_2/N_2 separation factor for sample M3 in the presence of 2 v/v % water concentration.

[Color figure can be viewed in the online issue, which is available at wileyonlinelibrary.com.]

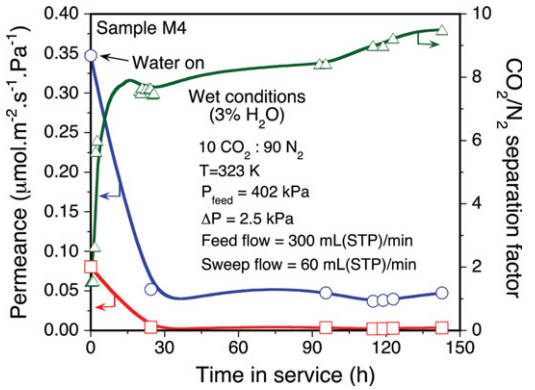

Figure 11. Time evolution of CO_2 and N_2 permeances and CO_2/N_2 separation factor for sample M4 in the presence of 3 v/v % water concentration.

[Color figure can be viewed in the online issue, which is available at wileyonlinelibrary.com.]

CO_2 emission reduction. Ideally, the CO_2 capture system should allow the removal of at least 85% of the CO_2 in the exhaust gas with a purity of 98% in the downstream permeate current with an energy consumption <4 GJ/t CO_2 avoided.

Input data and modeling details

As a case study, we consider here an application for CO_2 capture from an incineration plant. The input data have been obtained from an incineration plant operating in Rhône-Alpes (France) belonging to TREDI (Groupe Séché). The exhaust gas emitted from a low-temperature incinerator after catalytic NO_x reduction mainly consists of a mixture of CO_2, H_2O, and N_2 at the approximate molar ratio 10:15:75 at a temperature and pressure of 150°C and 101 kPa, respectively. The standard flowrate is about 120,000 Nm^3/h or 1.9 Mt/year. The solution here proposed would involve a first step of particle and water removal down to 10 v/v % and cooling down to 100°C to optimize the permeation performance of the MFI membranes. The resulting gas (molar composition CO_2:H_2O:N_2 10:10:80) would be then submitted to a membrane cascade system for capturing at least 85% (molar basis) of the emitted CO_2.

The general flowsheet of the membrane cascade system proposed in this study for postcombustion CO_2 capture from incinerators is depicted in Figure 13. The system consists of three membrane units with the permeate streams of the first and second units connected in series (i.e., the permeate of unit 1 feeds unit 2, whereas the permeate of unit 2 feeds unit 3). Some preliminary studies have suggested that at least 3 steps are needed to assure the desired threshold CO_2 molar fraction level of 0.98 at the outlet permeate stream after concentration given the separation properties of MFI membranes prepared in this study (see Ref. 49 for further details).

Assuming a quasi-isothermal regime, a modular membrane unit can be modeled using microscopic CO_2 and N_2 mass balances both in the lumen and in the permeate sides of the modules operating in counter-current mode. For the sake of simplicity, plug-flow (PF) regimes have been assumed to describe the hydrodynamics of the retentate (lumen) and permeate (shell) sides. The criteria for PF regime in tubular systems have been adapted from Rase.[50] At steady state, the set of Eqs. 3–5 is obtained[51,52]

- Microscopic mass balance in the retenate ($i = CO_2, N_2$)

$$-\frac{\partial(w_R\, x_i)}{S\,\partial z} - N_i\, a_m = 0 \tag{3}$$

- Microscopic mass balance in the permeate ($i = CO_2, N_2$)

$$-\frac{\partial(w_P\, y_i)}{S\,\partial z} + N_i\, a_m = 0 \tag{4}$$

- Transfer equation ($i = CO_2, N_2$)

$$w_P\, y_i(z) = \Pi_i(z)\, S(z)\, \left(P_i^R - P_i^P\right) \tag{5}$$

Boundary conditions: $z = 0 \rightarrow x_i = x_{i,in}$, $y_i = y_{in}$.

The model system defined by Eqs. 3–5 has been solved numerically through discretization using finite differences. The number of intervals (200) has been chosen to avoid any dependence of the simulation results on the discretization. The logarithmic partial pressure differences along the unit have been approached to linear differences in each finite element. The mixture CO_2 and N_2 permeances have been taken from Figures 4, 5, and 9C, respectively, in the absence and presence of moisture. The variation of both permeances with the feed composition has been explicitly taken into account in the calculations.

From a mathematical standpoint, a membrane cascade constituted by three units is characterized by 23 variables

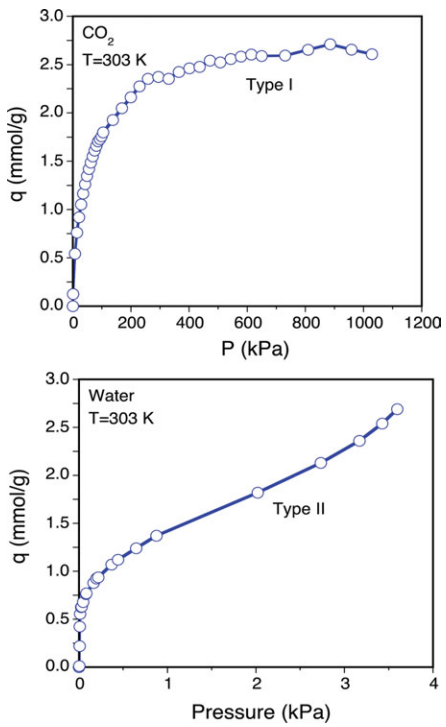

Figure 12. Comparison of CO_2 (top) and water (bottom) adsorption isotherm patterns on crushed Al-MFI-alumina fibers at 303 K.

The CO_2 isotherms have been corrected beyond 200 kPa to remove the contribution of the alumina support. [Color figure can be viewed in the online issue, which is available at wileyonlinelibrary.com.]

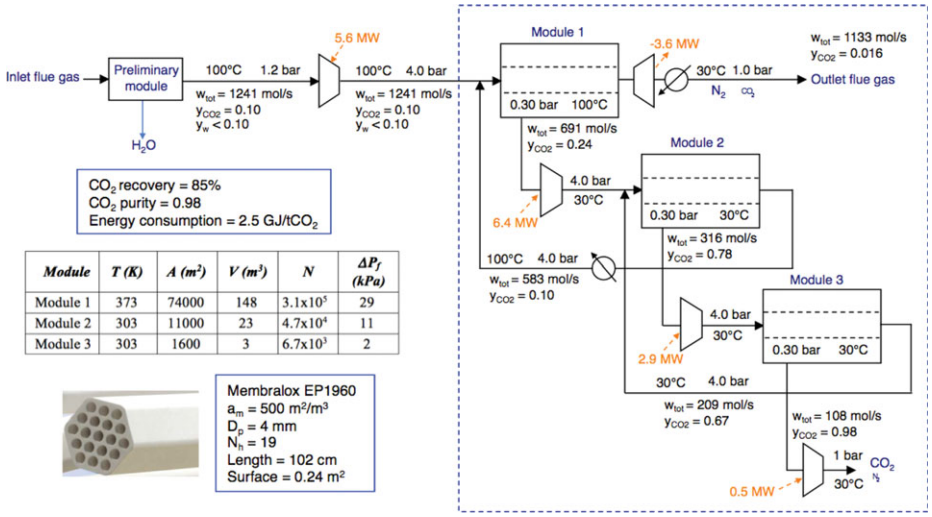

Figure 13. Flowsheet of a membrane cascade system for postcombustion CO_2 capture from a standard incineration plant together with the operation conditions and main characteristics of each unit.

[Color figure can be viewed in the online issue, which is available at wileyonlinelibrary.com.]

(seven total flowrates, seven CO_2 molar compositions, three retenate pressures, three permeate pressures, three surface areas, and six CO_2 and N_2 permeances) and 12 equations (3 CO_2 + 3 N_2 mass balances, and 3 CO_2 + 3 N_2 mass-transfer equations), leaving 17 degrees of freedom (the total flowrate and CO_2 molar fraction entering the cascade system, the CO_2 recovery, the CO_2 molar fraction at the permeate outlet of unit 3, the 3 retentate and 3 permeate pressures, the 6 CO_2 and N_2 permeances, the active surface of the first unit). Given the values for these degrees of freedom, the flowrate and composition in each stream, as well as the active surface of units 2 and 3, are univocal.

Unit 1 would operate at higher temperature (ca. 373 K) to avoid pore blocking upon direct contact with the inlet flue gas stream containing large amounts of water (concentration >10 v/v %), whereas units 2 and 3 would operate at 303–323 K. Figure 14 shows the simulated CO_2 molar fraction profiles in both the retentate and permeate sides of each module. Taking into account the low CO_2 concentration in the flue gas at the inlet of the separation system, the permeate stream should be kept under primary vacuum (>30 kPa) to enhance the CO_2 driving force across the membranes without increasing dramatically the retentate pressure. The concentrated CO_2 in the permeate stream would be further compressed and submitted subsequently to the second and third units to increase the CO_2 molar fraction up to 0.98 at the outlet of the third module. The concentrated CO_2 stream would be then pressurized at ambient pressure and then transported to the storage system.

Figure 13 also collects the related energy consumption and active surface for each membrane unit that would be required for 85% CO_2 capture and a final molar fraction of 0.98 at the outlet permeate stream. The maximum energy consumption can be estimated at 2.5 GJ/t CO_2 avoided (ca. 9.5 MW for 146 kt CO_2/year removal), this being attributed to the compression of the permeate streams coming from the first and second units from 30 to 404 kPa. The active surface required for separation decreases from a value of about 7.4 Ha for unit 1 to 1.1 and 0.16 Ha for units 2 and 3, respectively. The higher active surface for unit 1 is attributed to the much lower CO_2 permeance and separation capacity of MFI membranes in this unit due to the high CO_2 dilution level (cf. the values and trends indicated in Figure 13). However, the total active surface can be decreased by promoting the driving force within the membranes, either by increasing the retentate pressure or by decreasing the permeate pressure, in both cases at the expenses of an increase of the energy consumption. Figure 15 shows the evolution of the total active surface and the energy consumption as a function of the total retentate pressure, pointing out the selected operation conditions. Similar trends are observed when reducing the permeate pressure.

Number of membrane tubes and pressure drop

Given the active surfaces indicated in Figure 13, the number of membrane tubes can be estimated depending on their surface area. To carry out this estimation, we have chosen the Membralox EP1960 multichannel module manufactured by Pall-Exekia as standard basis. The main properties of this module are listed in Figure 13. We have already shown the optimal upscaling of our synthesis protocol for MFI membrane synthesis (see "Membrane preparation" section) on these supports.[51] The surface velocity in the membrane lumen has been established at 15 m/s to ensure optimal turbulence but at a reasonable axial pressure drop (<30 kPa, see Figure 13). Given the active surfaces computed at 404-kPa retenate pressure (7.4 + 1.1 + 0.16 Ha), these values translate into a demand of 31×10^5, 4.7×10^4, and 6.7×10^3 Membralox EP1960 modules for units 1, 2, and 3, respectively. The pressure drop along the membranes is estimated to <30 kPa for the former unit and <4 kPa for the other two. The suitability of the PF regime to describe the hydrodynamics inside the membranes is confirmed, since the condition $L/D_b = 10^5 > 100$ is fulfilled.[50]

Suitability of MFI-alumina membranes for module design: a technico-economical analysis

An orientative economic feasibility study of the technological solution proposed here for CO_2 capture (3-unit cascade system, see Figure 13) has been carried on the guidance of a previous study relying on a zeolite membrane reactor for liquid-phase DNPE production from *n*-pentanol

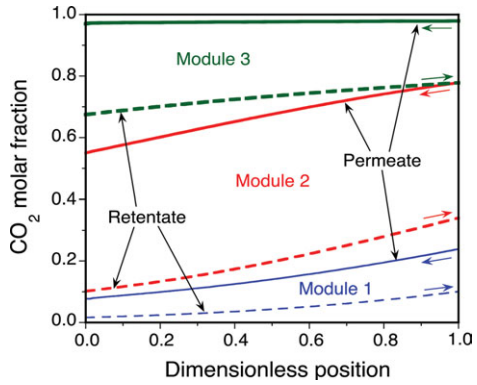

Figure 14. Simulation of the evolution of the molar fraction of CO_2 in the retentate (dashed curves) and permeate (straight curves) streams of the three module units with the dimensionless axial position for the MFI-alumina membranes prepared in this study.

[Color figure can be viewed in the online issue, which is available at wileyonlinelibrary.com.]

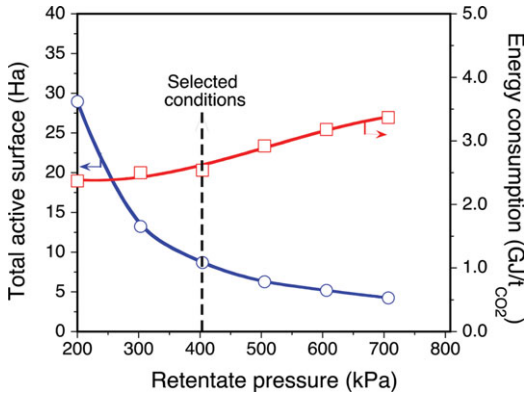

Figure 15. Comparative evolution of the total active surface and the energy consumption as a function of the retentate pressure at each unit using the input conditions indicated in Figure 13.

[Color figure can be viewed in the online issue, which is available at wileyonlinelibrary.com.]

etherification.[52] In terms of capital costs (Capex), our estimations reflect that, for 146 kt CO_2/year removal, about 90% of the cost of the plant would be ascribed to the membrane materials. The total cost ascribed to equipments would be about 84 M$, whereas the overall cost of the plant (equipment + installation) would reach 278 M$. The capital cost ascribed to membrane materials has been estimated by assuming a unit cost of about 1500 $/m^2 for membrane modules and a 10% increase due to MFI zeolite growth. Furthermore, the capital costs ascribed to compressors, heat exchangers, and condenser before the membrane cascade system have been estimated and upscaled using the Williams method, the costs being capitalized to present monetary units using Marshall & Swift correction factors.[53]

The analysis of the operation costs (OPEX) of the plant following conventional standards (see Table 2) reflects an annual cost about 50 M$ for 146 kt CO_2/year removal (5-Ha based plant with energy consumption ca. 10 MW/year). The higher contribution to the OPEX would be ascribed to membrane replacement (20% of the membrane surface per year) and power consumption, accounting for 35 and 7% of the overall costs, respectively. These costs would translate into a unit cost estimate for CO_2 capture at about 330 $/t CO_2 removed.

The estimation of the operation cost reduction of a membrane cascade system compared with a chemical absorption unit is not straightforward. However, according to the IPCC estimates, the implementation of a CO_2 capture unit in a coal power station for electrical production would involve a unit cost in the range 35–70 $/t CO_2 avoided for mature technologies (ethanolamine absorption), whereas a range of 150–180 $/t CO_2 avoided is proposed for new plants.[54] Some CO_2 capture cost estimates on highy permeable rubbery polymeric membranes match the first range.[10] The CO_2 removal costs obtained in our study are far from this latter interval according to the present state of development of membrane materials, with no scale economy benefits. A large-scale production of MFI membranes might involve a significant reduction of the CO_2 unit costs, approaching to the above stated intervals. As a matter of example, the unit cost would be reduced about 40% (ca. 200 $/t CO_2 avoided) if the unit cost for membrane production is reduced by a factor of 2. Moreover, a significant reduction of unit costs can be foreseen by changing the support material from α-alumina to mullite.

Conclusions

In this study, we have synthesized MFI-alumina membranes with nanocomposite architecture for CO_2/N_2 separation under realistic postcombustion CO_2 capture conditions (i.e., diluted CO_2 and presence of large amounts of water). At high water concentrations, beyond capillary condensation in small mesoporous defects, MFI membranes show a steady-state reduction of the gas permeance of about 40% for a water concentration of 10 v/v % at 373 K. The incorporation of water promotes however CO_2/N_2 separation factors, most probably due to defective pore blockage and formation of (bi)carbonate stable intermediates. The promising CO_2 permeation and separation properties of nanocomposite MFI-alumina membranes in the presence of water compared with other zeolite membrane materials (e.g., FAU-type membranes), combined with their hydrothermal stability and optimal reproducibility, make these materials potentially competitive for postcombustion CO_2 capture applications.

Table 2. Estimation of Operation Costs of the Plant Depicted in Figure 13 for 146 kt/Year Removal

Designation	Unit	Amount Per Year*	Unit Cost (k$/Unit)	OPEX (M$/Year)
Membrane replacement	m^2	14,000	1.6	16.5
Handworking (HW)†	Person	Direct: 45	35	1.5
		Indirect: 11	25	0.3
Staff	Person	2	65	0.1
Water (refrig.)	m^3	1.0×10^6	0.015	1
Water (service)	m^3	1.0×10^3	0.15	0.1
Electricity	kWh	9.1×10^7	0.045	4.2
Depreciation	–	4% Capex	–	3.4
Capital charges	–	2% Capex	–	5.6
Taxes	–	2% Capex	–	2.5
Insurance	–	3% Capex	–	5.6
Maintenance	–	2% Capex	–	5.6
Others	–	–	–	2.3
Total OPEX				48.6

*Capex = 3.3 × IC (investment cost) equipment (equipment + installation).
†Calculations carried out assuming a staff constituted of 70 people with the distribution: three technician:four specialist:five nonqualified personnel:two administrative:one staff member.

According to the technico-economical analysis provided in this study, MFI-alumina membranes could be promising candidates for postcombustion CO_2 capture from flue gases emitted from power and incineration plants if the support cost can be reduced. The high active surfaces demanded for high purification combined with their high unit cost make this technology however less competitive than conventional chemical absorption or some exploratory rubbery polymeric membranes. At a long-term horizon, scale economy effects and a reduction of the cost ascribed to the support might provide a significant reduction of the unit costs for membrane production, making membrane technology more competitive.

Acknowledgments

The authors would like to express their gratitude to the French Agence Nationale de la Recherche (ANR) for funding through the project ANR-07-PCO2-003.

Notation

A_b = membrane section, m^2
a_m = specific surface of the membranes, m^2/m^3
c_{sat} = gas concentration in the MFI crystals, mol/m^3
D_0^{∞} = Maxwell-Stefan diffusivity at zero coverage, m^2/s
D_p = inner diameter of membrane tubes, m
E_D = activation energy for surface diffusion, J/mol
L = length of membrane tubes, m
l = effective thickness, m
N = molar flux, mol m^{-2} s^{-1}
N_h^o = number of membranes in each unit
P = pressure, Pa
R = ideal constant of gases, 8.314 J mol^{-1} K^{-1}
T = temperature, K
w = molar flow, kmol/s
x = molar fraction infeed/retentate
y = molar fraction in permeate
z = axial position in the membranes, m

Greek letters

ΔH_{ads}^0 = standard adsorption enthalpy, J/mol
ΔS_{ads}^0 = standard adsorption entropy, J mol^{-1} K^{-1}
ε = porosity
η = dimensionless position in the membranes
ρ = density, kg m^{-3}
τ = tortuosity

Subscripts

in = initial
P = permeate
R = retentate

Acronyms

MFI = mobile five zeolite
MCM = mobile corporate material
MOF = metal organic framework
IC = investment cost
STP = standard conditions (101 kPa, 298 K)

Literature Cited

1. Richert P. Qualité de l'air et changement climatique: un même défi, une même urgence. Une nouvelle gouvernance pour l'atmosphère. In: *Special Report of the French Conseil National de l'Air in occasion of the 10th Anniversary of the French Loi de l'Air et l'utilisation rationnelle de l'énergie*, France, 2007.
2. Bredesen R, Jordal K, Bolland O. High-temperature membranes in power generation with CO_2 capture. *Chem Eng Process*. 2004;43:1129–1158.
3. Aresta M, Dibenedetto A. *Carbon dioxide fixation into organic compounds*. In: Aresta M, editor. *Carbon Dioxide Recovery and Utilization*. The Netherlands: Kluwer Academic Publishers, 2003:211–252.
4. Aaron D, Tsouris C. Separation of CO_2 from flue gas: a review. *Sep Sci Technol*. 2005;40:321–348.
5. Tagliabue M, Farrusseng D, Valencia S, Aguado S, Ravon U, Rizzo C, Corma A, Mirodatos C. Natural gas treating by selective adsorption: material science and chemical engineering interplay. *Chem Eng J*. 2009;155:553–566.
6. Li J-R, Kuppler RJ, Zhou H-C. Selective gas adsorption and separation in metal-organic frameworks. *Chem Soc Rev*. 2009;38:1477–1504.
7. Favre E. Carbon dioxide recovery from post-combustion processes: can gas permeation membranes compete with absorption? *J Membr Sci*. 2007;294:50–59.
8. Bernardo P, Drioli E, Golemme G. Membrane gas separation: a review/state of the art. *Ind Eng Chem Res*. 2009;48:4638–4663.
9. Hussain A, Hägg M-B. A feasibility study of CO_2 capture from flue gas by a facilitated transport membrane. *J Membr Sci*. 2010;359:140–148.
10. Merkel TC, Lin H, Wei X, Baker R. Power plant post-combustion carbon dioxide capture: an opportunity for membranes. *J Membr Sci*. 2010;359:126–139.
11. Huang Z, Li Y, Wen R, Teoh MM, Kulprathipanja S. Enhanced gas separation properties by using nano-structured PES-Zeolite 4A mixed matrix membrane. *J Appl Polym Sci*. 2006;101:3800–3805.
12. Husain S, Koros WJ. Mixed matrix hollow fiber membranes made with modified HSSZ-13 zeolite in polyetherimide polymer matrix for gas separation. *J Membr Sci*. 2007;288:195–207.
13. Reid BD, Ruiz-Trevino FA, Musselman IH, Balkus KJ Jr, Ferraris JP. Gas permeability properties of polysulfone membranes containing MCM-41 type mesoporous molecular sieves. *Chem Mater*. 2001;13:2366–2373.
14. Adams R, Carson C, Ward J, Tannenbaum R, Koros W. Metal organic framework mixed matrix membranes for gas separations. *Micropor Mesopor Mater*. 2010;131:13–20.
15. Coronas J, Santamaria J. Separations using zeolite membranes. *Sep Purif Methods*. 1999;28:127–177.
16. Julbe A. Zeolite membranes—synthesis, characterization and application (chapter 6). *Stud Surf Sci Catal*. 2007;168:181–219.
17. Caro J, Noack M. Zeolite membranes—recent developments and progress. *Micropor Mesopor Mater*. 2008;115:215–233.
18. Giroir-Fendler A, Peureux J, Mozzanega H, Dalmon J-A. Characterisation of a zeolite membrane for catalytic membrane reactor application. *Stud Surf Sci Catal*. 1996;101A:127–136.
19. Miachon S, Landrivon E, Aouine M, Sun Y, Kumakiri I, Li Y, Pachtová Prokopová O, Guilhaume N, Giroir-Fendler A, Mozzanega H, Dalmon J-A. Nanocomposite MFI-alumina membranes via pore-plugging synthesis: preparation and morphological characterisation. *J Membr Sci*. 2006;281:228–238.
20. Li Y, Pera-Titus M, Xiong G, Yang W, Landrivon E, Miachon S, Dalmon J-A. Nanocomposite MFI zeolite–alumina membranes via pore-plugging synthesis: genesis of the zeolite material. *J Membr Sci*. 2008;325:973–981.
21. Hyun SH, Song JK, Kwak BI, Kim JH, Hong SA. Synthesis of ZSM-5 zeolite composite membranes for CO_2 separation. *J Mater Sci*. 1999;34:3095–3103.
22. Kwak BI, Hyun SH, Kim GT. CO_2 separation characteristics of ZSM-5 composite membranes synthesized by the hydrothermal treatment. *J Mater Sci Lett*. 2001;20:1893–1896.
23. Guo H, Zhu G, Li H, Zou X, Yin X, Qiu S, Xu R, Yang W. Hierarchical growth of large-scale ordered zeolite silicalite-1 membranes with high permeability and selectivity for recycling CO_2. *Angew Chem Int Ed Engl*. 2006;45:7053–7056.
24. Sebastian V, Kumakiri I, Bredesen R, Menendez M. Zeolite membrane for CO_2 removal: operating at high pressure. *J Membr Sci*. 2007;292:92–97.
25. Kusakabe K, Kuroda T, Uchino K, Hasegawa Y, Morooka S. Gas permeation properties of ion-exchanged faujasite-type zeolite membranes. *AIChE J*. 1999;45:1220–1226.
26. Kusakabe K, Kuroda T, Murata A, Morooka S. Formation of a Y-type zeolite membrane on a porous-alumina tube for gas separation. *Ind Eng Chem Res*. 1997;36:649–655.
27. Kusakabe K, Kuroda T, Morooka S. Separation of carbon dioxide from nitrogen using ion-exchanged faujasite-type zeolite membranes formed on porous support tubes. *J Membr Sci*. 1998;148:13–23.
28. Hasegawa Y, Watanabe K, Kusakabe K, Morooka S. The separation of CO_2 using Y-type zeolite membranes ion-exchanged with alkali metal cations. *Sep Purif Technol*. 2001;22–23:319–325.
29. Hasegawa Y, Watanabe K, Kusakabe K, Morooka S. Influence of alkali cations on, permeation properties of Y-type zeolite membranes. *J Membr Sci*. 2002;208:415–418.

30. Weh K, Noack M, Sieber I, Caro J. Permeation of single gases and gas mixtures through faujasite-type molecular sieve membranes. *Micropor Mesopor Mater*. 2002;54:27–36.
31. Poshusta JC, Tuan VA, Falconer JL, Noble RD. Synthesis and permeation properties of SAPO-34 tubular membranes. *Ind Eng Chem Res*. 1998;37:3924–3929.
32. Poshusta JC, Tuan VA, Pape EA, Noble RD, Falconer JL. Separation of light gas mixtures using SAPO-34 membranes. *AIChE J*. 2000;46:779–789.
33. Li S, Falconer JL, Noble RD. SAPO-34 membranes for CO_2/CH_4 separation. *J Membr Sci*. 2004;241:121–135.
34. Li S, Martinek JG, Falconer JL, Noble RD, Gardner TQ. High-pressure CO_2/CH_4 separation using SAPO-34 membranes. *Ind Eng Chem Res*. 2005;44:3220–3228.
35. Li S, Falconer JL, Noble RD. Improved SAPO-34 membranes for CO_2/CH_4 separations. *Adv Mater*. 2006;17:2601–2603.
36. Tomita T, Nakayama K, Sakai H. Gas separation characteristics of DDR type zeolite membrane. *Micropor Mesopor Mater*. 2004;68:71–75.
37. van den Berg J, Zhu W, Gascon J, Kapteijn F. Separation and permeation characteristics of a DD3R zeolite membrane. *J Membr Sci*. 2008;316:35–45.
38. Cui Y, Kita H, Okamoto K-I. Preparation and gas separation performance of zeolite T membrane. *J Mater Chem*. 2004;14:924–931.
39. Poshusta JC, Noble RD, Falconer JL. Characterization of SAPO-34 membranes by water adsorption. *J Membr Sci*. 2001;186:25–40.
40. Himeno S, Tomita T, Suzuki K, Yoshida S. Characterization and selectivity for methane and carbon dioxide adsorption on the all-silica DD3R zeolite. *Micropor Mesopor Mater*. 2007;98:62–69.
41. Gu X, Dong J, Nenoff TM. Synthesis of defect-free FAU-type zeolite membranes and separation for dry and moist CO_2/N_2 mixtures. *Ind Eng Chem Res*. 2005;44:937–944.
42. Funke HH, Frender KR, Green KM, Wilwerding JL, Sweitzer BA, Falconer JL, Noble RD. Influence of adsorbed molecules on the permeation properties of silicalite membranes. *J Membr Sci*. 1997;129: 77–82.
43. Bernal MP, Coronas J, Menendez M, Santamaria J. Separation of CO_2/N_2 mixtures using MFI-type zeolite membranes. *AIChE J*. 2004;50:127–135.
44. Shin DW, Hyun SH, Cho CH, Han MH. Synthesis and CO_2/N_2 gas permeation characteristics of ZSM-5 zeolite membranes. *Micropor Mesopor Mater*. 2005;85:313–323.
45. Krishna R, van Baten JM. *In silico* screening of zeolite membranes for CO_2 capture. *J Membr Sci*. 2010;360:323–333.
46. Alshebani A, Pera-Titus M, Landrivon E, Schiestel Th, Miachon S, Dalmon J-A. Nanocomposite MFI-ceramic hollow fibres: prospects for CO_2 separation. *Micropor Mesopor Mater*. 2008;115:197–205.
47. Miachon S, Kumakiri I, Ciavarella P, van Dyk L, Fiaty K, Schuurman Y, Dalmon J-A. Nanocomposite MFI-alumina membranes via pore-plugging synthesis: specific transport and separation properties. *J Membr Sci*. 2007;298:71–79.
48. Alshebani A, Pera-Titus M, Yeung KL, Miachon S, Dalmon J-A. Influence of desorption conditions before gas separation studies in nanocomposite MFI-alumina membranes. *J Membr Sci*. 2008;314: 143–151.
49. Pera-Titus M, Alshebani A, Nicolas C-H, Miachon S, Dalmon J-A. Nanocomposite MFI-alumina membranes: high-flux hollow fibres for CO_2 capture from internal combustion vehicles. *Ind Eng Chem Res*. 2009;48:9215–9223.
50. Rase HF. *Chemical Reactor Design for Process Plants*, Vol.I. New York: Wiley, 1977.
51. Camus O, Perera S, Crittenden B, Delft YCV, Dick F, Meyerb O, Pex PAC, Kumakiri I, Miachon S, Dalmon J-A, Tennison S, Chanaud P. Ceramic membranes for ammonia recovery. *AIChE J*. 2006;52:2055–2065.
52. Pera-Titus M, Llorens J, Cunill F. Technical and economical feasibility of zeolite NaA membrane-based reactors in liquid-phase etherification reactions. *Chem Eng Process*. 2009;48:1072–1079.
53. Perry RH. *Perry's Chemical Engineering Handbook*, 6th ed. New York: McGraw-Hill, 1984.
54. Al-Juaied M, Whitemore A. *Realistic Costs for CO_2 Capture, Discussion Paper 2009-08*. Cambridge, Massachussets: Belfer Center for Science and International Affairs, July, 2009.

Manuscript received Jun. 14, 2011, revision received Aug. 2, 2011, and final revision received Oct. 27, 2011.